Received: 21 July 2022 | Revised: 30 September 2022 | Accepted: 18 October 2022

DOI: 10.1096/fba.2022-00082

RESEARCH ARTICLE

FASEB BioAdvances WILEY

FtsZ phosphorylation brings about growth arrest upon DNA damage in *Deinococcus radiodurans*

Reema Chaudhary[1,2] | **Shruti Mishra**[1,2] | **Ganesh K. Maurya**[3] | **Yogendra S. Rajpurohit**[1,2] | **Hari S. Misra**[1,2]

[1]Molecular Biology Division, Bhabha Atomic Research Centre, Mumbai, India

[2]Life Sciences, Homi Bhabha National Institute, Mumbai, India

[3]Mahila Maha Vidyalaya, Banaras Hindu University, Varanasi, India

Correspondence
Hari S. Misra, Molecular Biology Division, Bhabha Atomic Research Centre, Mumbai- 400094, India.
Email: hsmisra@barc.gov.in

Abstract

The polymerization/depolymerization dynamics of FtsZ play a pivotal role in cell division in the majority of the bacteria. *Deinococcus radiodurans*, a radiation-resistant bacterium, shows an arrest of growth in response to DNA damage with no change in the level of FtsZ. This bacterium does not deploy LexA/RecA type of DNA damage response and cell cycle regulation, and its genome does not encode SulA homologues of *Escherichia coli*, which attenuate FtsZ functions in response to DNA damage in other bacteria. A radiation-responsive Ser/Thr quinoprotein kinase (RqkA), characterized for its role in radiation resistance in this bacterium, could phosphorylate several cognate proteins, including FtsZ (drFtsZ) at Serine 235 (S235) and Serine 335 (S335) residues. Here, we reported the detailed characterization of S235 and S335 phosphorylation effects in the regulation of drFtsZ functions and demonstrated that the phospho-mimetic replacements of these residues in drFtsZ had grossly affected its functions that could result in cell cycle arrest in response to DNA damage in *D. radiodurans*. Interestingly, the phospho-ablative replacements were found to be nearly similar to drFtsZ, whereas the phospho-mimetic mutant lost the wild-type protein's signature characteristics, including its dynamics under normal conditions. The kinetics of post-bleaching recovery for drFtsZ and phospho-mimetic mutant were nearly similar at 2 h post-irradiation recovery but were found to be different under normal conditions. These results highlighted the role of S/T phosphorylation in the regulation of drFtsZ functions and cell cycle arrest in response to DNA damage, which is demonstrated for the first time, in any bacteria.

KEYWORDS

cell cycle regulation, Deinococcus, FtsZ dynamics, non-canonical DNA damage response, Radioresistance, S/T phosphorylation

1 | INTRODUCTION

The bacterial cell division is orchestrated by the coordinated functions of an array of cell division proteins called the divisome and genome segregation proteins called the segrosome. The mechanisms of cell division have been extensively studied in both Gram-negative and Gram-positive bacteria such as *Escherichia coli*, *Bacillus subtilis*, *Streptococcus pneumoniae*, *Staphylococcus aureus*, *Mycobacterium tuberculosis* and *Caulobacter crescentus*.[1] The assembly of divisome at the mid-cell position is both spatially and temporally regulated.[2,3] FtsZ, a tubulin homologue and a key protein in the bacterial cell division, undergoes GTP-dependent polymerization–depolymerization dynamics, and it forms the FtsZ-ring (Z-ring) largely at the mid-cell position.[4–6] FtsZ exists in two conformations: an open conformation observed in the filaments and a closed conformation in the monomeric form.[7] The structural and functional properties of FtsZ protein are influenced by other proteins through protein–protein interactions. For example, the FtsA, ZipA and Zap proteins help in anchoring and stabilizing the Z-ring at the mid-cell position, whereas the MinCDE, SlmA and Noc proteins prevent the formation of the Z-ring at the undesired sites, *although* through different mechanisms. The Z-ring stability at the cytoplasmic membrane is dependent on the interaction with other proteins and also serves as a scaffold for the recruitment of downstream proteins for the septal peptidoglycan biosynthesis.[8,9] The GTP-binding pocket is found to be conserved in FtsZ across different bacterial species and is required for the polymerization of FtsZ. The dynamics of FtsZ polymerization/depolymerization play a crucial role in bacterial cell division.[8,10–13] In response to DNA damage, the functions of FtsZ are attenuated by SOS response proteins such as SulA in *E. coli*,[14] YneA in *B. subtilis*,[15] Rv2719c in *M. tuberculosis*[16] and SidA in *C. crescentus*.[17]

Deinococcus radiodurans is an extraordinary radiation-resistant bacterium that divides into perpendicular planes. It can tolerate the mutagenic effects of several DNA-damaging agents, including radiation and desiccation.[18–20] *D. radiodurans* shows an arrest of the growth in response to γ-irradiation.[21] The transcriptome analyses showed changes in the expression kinetics of DNA repair genes[22,23] and protein recycling in the cells recovering from γ-irradiation.[24] Notably, there was no change in the levels of some putative cell division proteins, including FtsZ, during post-irradiation recovery (PIR).[21] *D. radiodurans* lacks the LexA-/RecA-type DNA damage response and cell cycle regulation[25] and its genome does not encode the FtsZ attenuator such as SulA or its homologues. How this bacterium regulates FtsZ functions and the cell cycle is intriguing. A γ-radiation-responsive Ser/Thr quinoprotein kinase encoded on an ORF DR_2518 (named RqkA) has been characterized in this bacterium for its role in radiation resistance and DNA double-strand break (DSB) repair.[26] RqkA phosphorylates a large number of cognate proteins, including those involved in DNA repair and cell division, and thus the possibility of RqkA regulating the global response to DNA damage and cell cycle would be interesting to investigate. Here, we provided evidence that the mimicking phosphorylation of deinococcal FtsZ (drFtsZ) at serine 235 (S235) and serine 335 (S335) positions by RqkA during PIR attenuates the functions of drFtsZ, including the arrest of its polymerization/depolymerization dynamics in *D. radiodurans*. Although FtsZ phosphorylation has been reported in canonical SOS response conferring bacteria,[27] the role of S/T phosphorylation in FtsZ by a DNA damage-responsive eSTPK and its effect on the γ-radiation stressed growth is being shown for the first time in any bacteria. The findings reported in this work may form a basis for proposing an STPK-based mechanism of DNA damage response and cell cycle regulation in prokaryotes as well.

2 | MATERIALS AND METHODS

2.1 | Bacterial strains, plasmids and materials

D. radiodurans R1 (ATCC13939) was a kind gift from Professor J. Ortner, Germany.[28] *Escherichia coli* strains DH5α and NovaBlue were used for cloning and maintenance of the plasmids, and *E. coli* strain BL21 (DE3) pLysS was used for the expression of recombinant proteins. *E. coli* was grown in Luria Bertini (LB) broth, and *D. radiodurans* was grown in TGY medium (1% Bacto tryptone, 0.1% glucose and 0.5% yeast extract) with shaking at 180 rpm at 37°C and 32°C, respectively. *E. coli* harbouring the recombinant expression vectors and their derivatives were grown in the presence of antibiotics, as required. Molecular biology-grade chemicals and enzymes were purchased from Merk Inc. and New England Biolabs, USA.

2.2 | Site-directed mutagenesis using overlap-PCR

Phospho-site mapping of drFtsZ incubated with RqkA kinase has shown that serine residues located at the 235 (S235) and 335 (S335) positions are phosphorylated.[29] To study the effect of phosphorylation on the functional aspects of drFtsZ, the S235 and S335 were substituted with alanine (phospho-ablative) or aspartic acid

(phospho-mimetic) in different combinations (Table 1). Overlapping primers were designed to mutate S235 and/or S335 of drFtsZ. The *ftsZ* gene segments were amplified using two sets of primers, forward *ftsZ* and reverse $ftsZ^{S235A}$ and forward $ftsZ^{S235A}$ and reverse *ftsZ* primers, in separate reactions. These gene segments were used as a template for an overlap PCR to generate a full-length *ftsZ* gene carrying the desired mutation by using the *ftsZ* forward and reverse primers containing restriction sites. For hybridization and an extension of the overlapping strands, two PCR cycles were run as follows: denaturation (3 min), 20 cycles of denaturation (30 s, 95°C), annealing (2 min, required temperature), extension (1 min 10 s, 72°C) followed by an extension of 5 min at 72°C and then the reaction was subjected to another PCR cycle of denaturation (2 min), 20 cycles of denaturation (30 s, 95°C), annealing (35 s, required temperature) and extension (1 min 10 s, 72°C) followed by a final extension of 10 min at 72°C. The *ftsZ*-mutant alleles were cloned in pET28a (+) at *Nde*I and *Bam*HI, yielding pETZS235A, pETZS235D, pETZS335A and pETZS335D. The double phospho-mutants were generated using pETZS335A and pETZS335D as templates using overlapping primers as shown in Table 1, and double mutants bearing recombinant plasmids such as pETZAA, pETZAD, pETZDA and pETZDD were obtained (Table 1). The recombinant plasmids were further transformed into *E. coli* BL21 cells, and the protein expression was ascertained by SDS-PAGE.[29]

The coding sequences for drFtsZ, $FtsZ_{AA}$ and $FtsZ_{DD}$ were PCR amplified using the required primers from pETZ,[21] pETZAA and pETZDD plasmids, respectively. These products were cloned in pDSW208[30] at *Bam*HI and *Xba*I to obtain pDsZ, pDsZAA and pDsZDD plasmids. The coding sequences for translation fusion of drFtsZ, $FtsZ_{AA}$ and $FtsZ_{DD}$ with GFP were PCR amplified from pDsZ, pDsZAA and pDsZDD, respectively, and cloned in pRadgro[31] at *Apa*I-*Eco*RV to yield pRGZGFP, $pRGZ_{AA}$GFP and $pRGZ_{DD}$GFP plasmids, which were further transformed in *D. radiodurans* using the protocol as described earlier.[32]

2.3 | Purification of recombinant proteins

The recombinant drFtsZ (~39 kDa) and its mutant derivatives expressed in the *E. coli* BL21 cells were purified to near homogeneity using the protocol as described.[21] In brief, an overnight-grown culture expressing the recombinant protein was diluted at 1:100 in fresh LB broth containing 25 μg/ml kanamycin. To this, 0.5 mM isopropyl-β-D-thio-galactopyranoside (IPTG) was added in exponentially growing cells, and these cells were harvested after 3 h post-induction. The cell pellet was suspended in buffer A (20 mM Tris–HCl, pH 7.6, 250 mM NaCl) containing 10 mM imidazole, 0.5 mg/ml lysozyme, 1 mM PMSF, 0.03% NP-40, 0.03% Triton X-100 and 10% glycerol and incubated at 37°C for 30 min. To this, the protease inhibitor cocktail was added, and the cells were sonicated for 10 min at 15 s pulses with intermittent cooling for 30 s at 25% amplitude. The cell lysate was centrifuged at 11,000 rpm for 30 min at 4°C. The cell-free extract was loaded onto $NiCl_2$ charged fast-flow chelating sepharose column (GE Healthcare) pre-equilibrated with buffer A. The column was washed with 20 column volumes of buffer A containing 50 mM imidazole till proteins stop coming from the column. Recombinant proteins were eluted with buffer A containing 100, 200, 250, and 300 mM imidazole. The fractions were analyzed by SDS-PAGE, and fractions containing nearly pure proteins were pooled and concentrated using 10 kDa cut-off spin columns and then centrifuged at 14,000 rpm for 60 min to remove aggregates, if any. The concentrated protein was dialysed against buffer A and subjected to further purification using the gel-filtration sepharose column (GE Healthcare) in AKTA pure. The fractions were analyzed by SDS-PAGE, and those containing nearly pure proteins were pooled, and the histidine tag was removed with Factor Xa using the manufacturer's protocol. The mixture was concentrated using 10 kDa cut-off spin columns and then centrifuged at 14,000 rpm for 60 min. The protein in the supernatant was dialysed in buffer A containing 10 mM Tris–HCl pH 7.6, 250 mM NaCl, 20% glycerol and 1 mM PMSF and stored at −20°C.

2.4 | Biochemical assays

The GTPase activity was measured as the release of [^{32}P]-αGDPs from [^{32}P]-αGTPs by thin-layer chromatography (TLC).[21] In brief, proteins in different concentrations were pre-incubated in 20 μl polymerization buffer (PB) (20 mM Tris–HCl, pH 7.5, 75 mM KCl) supplemented with $MgCl_2$ as required at 37°C for 10 min before the reaction was initiated with [α^{32}P]-GTP. Reaction mixtures were further incubated at 37°C for 20 min. The reaction was terminated by the addition of 10 mM EDTA solution. The reaction mixture was now spotted on the PEI Cellulose F^+ TLC sheets. Spots were air-dried, and mixtures were separated on the solid support in a buffer (0.75 M KH_2PO_4/H_3PO_4 [pH 3.5]). TLC sheets were exposed to X-ray films in a light-proof cassette. Autoradiograms were developed and images were analyzed using Image-J and GraphPad Prism 6 software. The GTPase activity was also measured using the malachite-green assay as per the manufacturer's protocol (Sigma-MAK113). The binding of GTP to recombinant proteins was checked as described earlier.[33]

TABLE 1 List of plasmids, strains and primers used in this study

Plasmids			
S. No	**Plasmids**	**Description**	**Source**
1	pET28a(+)	~5.3 kb plasmid; N-terminal 6XHis tag (Kan^R)	Novagen Inc
2	pDSW208	pDSW208-MCS-*gfp* (fusion vector) (Amp^R)	Ref. 30
3	pRadgro	pRAD1, *groESL* promoter (261 bp) of *D. radiodurans* at *Bgl*II-*Xba*I site, ~6.5 kb, AmpR	Ref. 31
4	pETZ	pET28a(+) carrying *ftsZ* at NdeI and BamHI	Ref. 21
5	pETZAA	pET28a(+) carrying *ftsZ* with mutation at S235A and S335A at NdeI and *Bam*HI	This study
6	pETZDD	pET28a(+) carrying *ftsZ* with mutation at S235D and S335D, at NdeI and *Bam*HI	This study
7	pETZAD	pET28a(+) carrying *ftsZ* with mutation at S235A and S335D, at NdeI and *Bam*HI	This study
8	pETZDA	pET28a(+) carrying *ftsZ* with mutation at S235D and S335A at NdeI and *Bam*HI	This study
9	pETZS235A	pET28a(+) carrying *ftsZ* with mutation at 235th serine codon to alanine codon at NdeI and *Bam*HI	This study
10	pETZS335A	pET28a(+) carrying *ftsZ* with mutation at S335A at NdeI and *Bam*HI	This study
11	pETZS235D	pET28a(+) carrying *ftsZ* with mutation at S235D at NdeI and *Bam*HI	This study
12	pETZS335D	pET28a(+) carrying *ftsZ* with mutation at S335D at NdeI and *Bam*HI	This study
13	pDsZ	pDSW208 with *ftsZ* at *Bam*HI-*Xba*I to give *ftsZ-gfp*(Amp^R)	Ref. 21
14	pVHZGFP	pVHSM containing *ftsZ-gfp* at *Sac*I-*Afl*II site, ~11.7 kb, $Spec^R$	Ref. 21
15	pDsZAA	pDSW208 with $ftsZ_{AA}$ at *Bam*HI-*Xba*I to give *ftsZ-gfp*	This study
16	pDsZDD	pDSW208 with $ftsZ_{DD}$ at *Bam*HI-*Xba*I to give *ftsZ-gfp*	This study
17	pRGZGFP	pRadgro carrying *ftsZ-gfp* from pDSZ at *Apa*I & *Eco*RV	This study
18	$pRGZ_{DD}GFP$	pRadgro carrying $ftsZ_{DD}$-*gfp* at *Apa*I & *Eco*RV	This study
19	$pRGZ_{AA}GFP$	pRadgro carrying $ftsZ_{AA}$-*gfp* at *Apa*I & *Eco*RV	This study
20	pNKZ	pNOKOUT containing upstream (~1.0 kb) and downstream (~1.1 kb) sequences of *ftsZ*, ~6.7 kb, Amp^R/ Kan^R	This study
Strains			
Sl. No.	**Strains**	**Genotype and phenotype**	**Source**
1	*Escherichia coli* NovaBlue	*end*A1 *hsd*R17(r_{K12}^{-} m_{K12}^{+}) *sup*E44 *thi-1 rec*A1 *gyr*A96 *rel*A1*lac*F"*[pro*A^+B^+*lac*$I^qZ\Delta$M15::T*n*10] (Tet^R)	NEB Inc.
2	*E. coli* BL21	F^- *ompT gal dcm lon hsd*S_B($r_B^-m_B^-$) λ(DE3 [*lacI lacUV5-T7p07 ind1 sam7 nin5*]) [*malB*$^+$]$_{K\text{-}12}$(λ^S) pLysS[*T7p20 ori*$_{p15A}$](Cm^R)	Lab Stock
3	*Deinococcus radiodurans*	Wild type strain ATCC13939	Lab Stock
4	△*ftsZ*	*ftsZ* gene replaced with kanamycin resistance gene cassette (*nptII*^{R}) complemented with pVHZGFP	This study

TABLE 1 (Continued)

Oligonucleotides			
S. No	**Primers**	**Oligonucleotide Sequences**	**Purpose**
1	pETZFw	5′GGAATTCCATATGCAAGCAGCCAGAATTCGCGT 3′	For cloning in pET plasmids
2	pETZRw	5′ CGGGATCCTTACTGTCCGCCGACGT 3′	
3	HisRedFw	5′CGGAGCTCGGGCCCCACCACCACCACCACCACCATGCCTGCAGGTCG 3′	For construction of pRGZGFP, $pRGZ_{AA}$GFP $pRGZ_{DD}$GFP
4	RedRw	5′ GGATATCTAGACTCGAGGCCGCTACAG 3′	
5	pDSFw	5′GGAATTCCATATGCAAGCAGCCAGAATTCGCGT 3′	For construction of pDsZ, pDsZAA, pDsZDD
6	pDSRw	5′ CGTCTAGACTGTCCGCCGACGT 3′	
7	FZ235AFw	5′GGAAGCTGCCATGGCAGCCATTCACTCGCCG 3′	For S235A in wild type and ZS335A, ZS335D background
8	FZ235ARw	5′CGGCGAGTGAATGGCTGCCATGGCAGCTTCC 3′	
9	FZ335AF	5′ CAGGGCGGCTACGGCGCAGGTCTGGTGCGCCC 3′	For S335A mutagenesis
10	FZ335AR	5′ GGGCGCACCAGACCTGCGCCGTAGCCGCCCTG 3′	
11	FZ335DF	5′ CAGGGCGGCTACGGCGACGGTCTGGTGCGCCC 3	For S335D mutagenesis
12	FZ335DR	5′ GGGCGCACCAGACCGTCGCCGTAGCCGCCCTG 3′	
13	FZ235DFw	5′GGAAGCTGCCATGGACGCCATTCACTCGCCG 3′	For S235D in wild type and ZS335A, ZS335D background
14	FZ235DRw	5′CGGCGAGTGAATGGCGTCCATGGCAGCTTCC 3′	
15	nptIIFw	5′GCACGGTGGCCGAGTGG 3′	Diagnostic PCR
16	nptIIRw	5′GTCAGCGTAATGCTCTG 3′	
17	ZUPFw	5′GCGGGCCCATGAGAGAAAAC3′	pNKZ, Diagnostic PCR
18	ZUPRw	5′GGATATCTCAGAACCAGTCGC3′	
19	ZDNFw	5′CGGGATCCAGTAGCGGTCCTTCTGT3′	pNKZ, Diagnostic PCR
20	ZDNRw	5′GCTCTAGATACAGAAGGCGCGGCG3′	

In brief, 100 nM 2′/3′-O-(N-methyl-anthraniloyl) guanosine 5′ triphosphate, trisodium salt (Mant-GTP) (M12415; Invitrogen) was incubated with 5 μM of wild type and mutant proteins separately in binding buffer (Tris–HCl, pH 7.6; 50 mM, KCl; 30 mM and $MgCl_2$; 0.5 mM) and, Mant-GTP binding to protein was monitored as the emission using JASCO spectrofluorometer FP-8500.

2.5 | Biophysical characterization

The quality of purified recombinant proteins was assayed by Circular Dichroism (CD) spectroscopy as described earlier.[34] In brief, 0.5 μM protein was diluted in a buffer containing 20 mM Tris (pH 7.6) and 150 mM NaCl and the spectra were recorded using a CD spectrophotometer (Biologic Spectrometer MOS-500).

Further, the sedimentation assay was carried out using a modified protocol as described earlier.[21] In brief, 5 μM of the purified recombinant drFtsZ and phospho-mutant derivatives were pre-incubated in polymerization buffer (PB) supplemented with 5 mM $MgCl_2$ followed by the addition of 1 mM GTP/GDP as required. In all these experiments, the protein was pre-incubated in PB buffer with 5 mM $MgCl_2$ at 37°C for 5 min and 1 mM GTP or GDP and further incubated for 20 min at 37°C. The reaction mixtures were centrifuged at 16,000 g for 30 min at room temperature. The pellet and supernatants were separated and analysed on 12% SDS-PAGE. Protein bands were visualized by Coomassie Brilliant Blue staining. Images were analysed using ImageJ and GraphPad Prism 6 software.

The polymerization dynamics of phospho-mutants of drFtsZ were monitored by 90° dynamic light scattering (DLS) as described earlier.[35] In brief, all the solutions used in this study were passed through a 0.22 μm filter, and the protein was centrifuged at 14,000 rpm for 60 min at 4°C. The DLS spectra were recorded with 5 μM purified proteins incubated with and without 1 mM GTP in PB buffer for 5 min at 37°C using a Malvern Zetasizer. Data were recorded for 20 min at an interval of 30 s, and light-scattering intensity in kilocounts per sec (kcps) was plotted against time using GraphPad software.

For transmission electron microscopy, 5 μM of the wild-type and mutant proteins were incubated in polymerization buffer (PB buffer; 50 mM Tris–HCl, pH 7.6, 50 mM KCl and 5 mM $MgCl_2$) for 5 min at room temperature followed by 15 min incubation at 37°C in the presence of 1 mM GTP. For mounting, the carbon-coated TEM grids were charged under UV light, and reaction mixtures were transferred on the grids followed by staining with a 2% uranyl acetate solution. The grids were washed with Milli-Q water and left for drying at room temperature overnight, then observed at a magnification of 10,000× (120 keV) using a transmission electron microscope JEM-1400 (JEOL).

2.6 | Confocal microscopy

Confocal microscopy was performed on an IX3SVR motorized platform using an Olympus IX83 inverted microscope with the laser beams focused on the back focal plane of a 100 × 1.40 NA oil-immersion apochromatic objective lens (Olympus, Inc). The intensity and time sequence of laser illumination at the sample were tuned using an installed version of Fluoview™ software. The series of Z planes were acquired at every 400 nm. Fluorescence emission was collected through a DM-405/488 dichroic mirror and the corresponding single-band emission filters.

For fixed cell imaging, the bacterial cells were grown to the mid-log or late-log phase in LB or TYG broth, fixed with 4% paraformaldehyde for 10 min on ice, and washed two times with phosphate-buffered saline (PBS; pH 7.4). These cells were stained with DAPI (0.5 μg/μl) for 10 min on ice and then washed three times with PBS. After washing, the cells were resuspended in PBS, mounted on a 1% agarose bed on glass slides, and the samples were observed. For image analysis, the 200–300 cells were taken from at least two separate microscopic fields captured in two independent experiments and analysed for required attributes. The image analysis and other cell parameters were measured using automated cellSens software. The data obtained were subjected to Student *t* test analysis using statistical programs of GraphPad Prism 6. For time-lapse microscopy, the cells in the exponential phase were rinsed in PBS before imaging. Cells were deposited on an agarose pad made with 2X-TYG and impregnated with air holes to oxygenate the cells. The 3D images (Z planes were acquired every 400 nm) were acquired every 45–60 min for a period of 4–5 h using very low 488 nm laser power. Images were processed using the cellSens software and Adobe Photoshop 7.0.

For fluorescence recovery after photobleaching (FRAP) experiments, deinococcal cells expressing pRGZGFP, $pRGZ_{AA}GFP$ and $pRGZ_{DD}GFP$ in exponential phase were exposed to a 6 kGy dose of γ-radiation using GC-5000, whereas control cells (unirradiated) were kept on ice. After γ-irradiation, both unirradiated (UI) and irradiated (I) cells expressing $FtsZ_{WT}$, $FtsZ_{AA}$ and $FtsZ_{DD}$ were collected at 0 h and 2 h of post-irradiation recovery. The cells were processed for confocal microscopy as described above. The region of interest was exposed to a laser bleach pulse of 35 to 45 ms followed by the acquisition of recovery for 30–40 s at low laser power. The fluorescence intensities in the bleached and other regions at each time point were extracted using the cellSens software and exported to

Excel 2013. For each spot, the background intensity was subtracted and a correction factor was applied for overall photobleaching of the region of interest during observation using easy-FRAP software. Recovery half-times were determined by performing a non-linear regression fit of the intensity of the bleached region over time using GraphPad software.[36]

2.7 | Immunoblotting of total cellular proteins

Immunoblotting of total proteins was carried out as described earlier.[32] In brief, only *E. coli* cells and *E. coli* expressing pDSW208, pDsZ, pDsZAA and pDsZDD were grown at 37°C, and *D. radiodurans* and its variants harbouring pRadgro, pRGZGFP, pRGZ$_{AA}$GFP and pRGZ$_{DD}$GFP were grown at 32°C. The optical density of bacterial cultures was adjusted to 1.0, and cells were centrifuged. The cell pellets were washed with 1X PBS and lysed at 95°C for 15 min in equal volumes of TE buffer (10 mM Tris–HCl pH 8.0 and 1 mM EDTA) and 2X Laemmli buffer. The equal amount of protein was run on 12% SDS-PAGE and blotted on PVDF membrane using a BioRad semi-dry blot machine. Blots were hybridized with monoclonal antibodies against GFP and polyclonal antibodies against drFtsZ followed by anti-mouse and anti-rabbit alkaline-phosphatase-conjugated antibodies, respectively, and signals were developed using NBT-BCIP (Roche).

2.8 | Construction of conditional null mutant of ftsZ

The recombinant plasmid pNKZ was constructed for the deletion of *ftsZ* (DR_0631) from chromosome I in *D. radiodurans*. For that, ~1 kb of upstream and downstream regions of the coding sequence of drFtsZ was PCR amplified using sequence-specific primers (Table 1). PCR products were digested with the required restriction enzymes and cloned into the pNOKOUT plasmid. The upstream and downstream fragments of *ftsZ* were cloned at *Apa*I-*Eco*RI and *Bam*HI-*Xba*I sites in pNOKOUT (Kan^R), respectively, to give pNKZ. For the expression of drFtsZ *in trans*, the recombinant plasmid pVHZGFP expressing FtsZ-GFP under the '*Spac*' promoter was used, and replacement of the chromosomal copy of *ftsZ* with *nptII* using pNKZ was achieved as described earlier.[32] The wild-type cells were also transformed with the vector backbone pVHSM as a control. The homogenous replacement of the target sequence with the *nptII* cassette was confirmed by diagnostic PCR using gene-specific primers as given in Table 1 *ftsZ* with the expressing cassette of *nptII* was achieved in the presence of an episomal copy; pVHZGFP, resulting in a genotype of *ftsZ*::*nptII* (hereafter referred to as *ΔftsZ*). The recombinant plasmids, pRGZGFP, pRGZ$_{AA}$GFP and pRGZ$_{DD}$GFP, were also transformed into *ΔftsZ* to monitor the effect of phospho-ablative and phosphomimetic replacements on the physiological functions of FtsZ in vivo. The wild-type and other derivatives expressing FtsZ on plasmids were grown in the presence of respective antibiotics and exposed to γ-radiation (6 kGy), whereas unirradiated cells were kept on ice and their growth kinetics were monitored using a Synergy H1 Hybrid multi-mode microplate reader, Biotek for overnight at 32°C. The corresponding growth rates were also calculated and analysed for statistical significance and plotted using GraphPad Prism 6 software.

3 | RESULTS

3.1 | The phosphorylation sites Serine 235 and Serine 335 of drFtsZ are non-conserved in FtsZ homologues

The FtsZ homologues are largely conserved across the bacteria and are structurally divided into three domains; the N-terminal domain, the globular conserved core domain and the C-terminal domain containing linker and variable regions (Figure 1A [i]). Multiple sequence alignment of FtsZ from different bacteria revealed that deinococcal FtsZ (drFtsZ) is ~41.77% identical and ~56.61% similar to *B. subtilis's* FtsZ (Figure 1A [ii]). The positional conservation of serine residues at the 235th and 335th position of drFtsZ was analysed across the FtsZ homologues of different bacteria and was found to be non-conserved (Figure 1A [iii]). The structure of drFtsZ was modelled using I-TASSER and refined using ModLoop and RAMPAGE server (Figure 1B [i]). The model structure was aligned with the structure of FtsZ of *B. subtilis* (PDB ID: 2VXY) using TM-Align and Pymol (Figure 1B [ii]). The aligned models show an RMS value of 1.36 and a TM score of 0.96034, indicating that both structures are highly identical. Earlier, the RqkA phosphorylation of S235 and S335 residues in drFtsZ was demonstrated.[29] We checked the position of these residues in the 3D structure of drFtsZ. We observed that S235 lies in close proximity to the GTP binding pocket while S335 appears to be present in the neighbourhood of the intrinsically disordered peptide (IDP) region of the drFtsZ. The S235 and S335 were replaced with alanine and aspartate in single and double combinations as shown in Figure 1C.

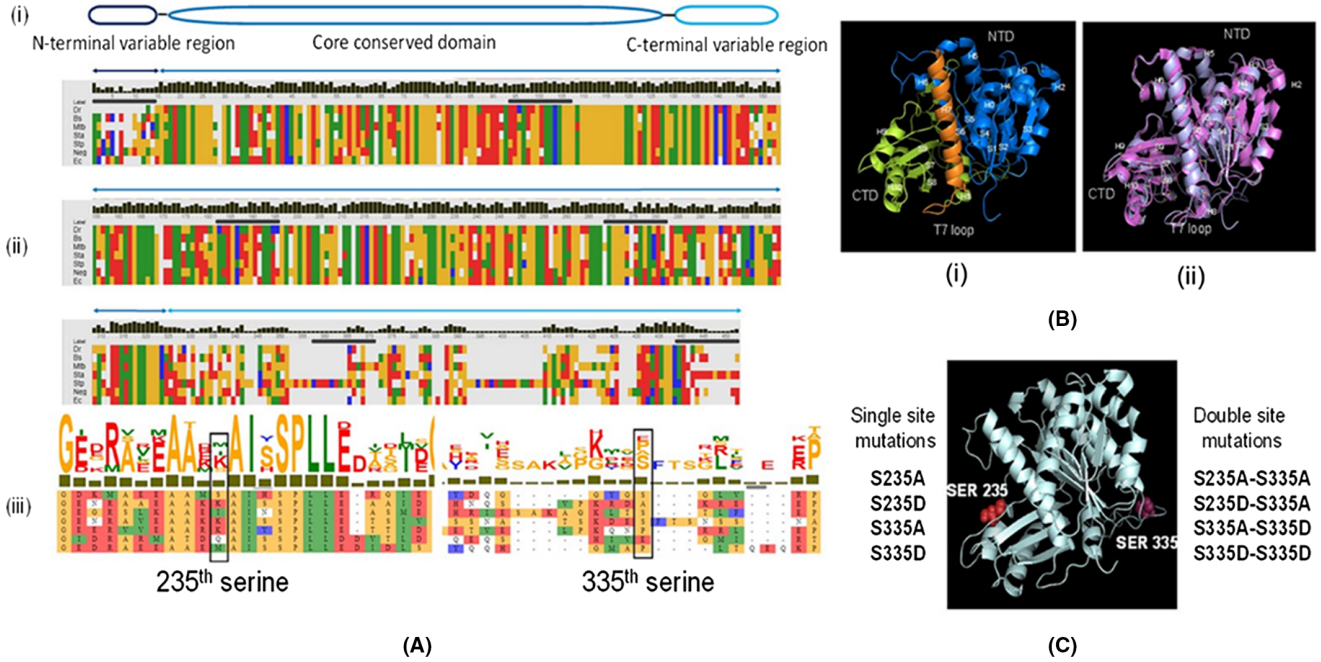

FIGURE 1 The sequence analysis, structural prediction and representation of mutations in drFtsZ. The general representation of the domains and regions of FtsZ (I), the multiple sequence alignment using the sequence of FtsZ from different bacterial species such as *Deinococcus radiodurans* (Dr), *Bacillus subtilis* (Bs), *Mycobacterium tuberculosis* (Mtb), *Staphylococcus aureus* (Sta), *Streptococcus pneumoniae* (Stp), *Neisseria gonorrhoeae* (Neg) and *Escherichia coli* (Ec) is performed using MSAProbs webserver (ii), 235th and 335th serine residues are shown separately where it indicates the less order of conservation at these residues across several bacterial species (iii) (A). Structure of deinococcal FtsZ (drFtsZ) was modelled using I–Tasser and ModLoop server where NTD (N-terminal domain), T7-loop and CTD (C-terminal domain) are labelled (i), The structure of drFtsZ overlapped with bsFtsZ (*B. subtilis* FtsZ; PDB ID 2VAM) (ii) (B). The two serine residues that were mapped as phospho-sites in drFtsZ are mutated to alanine and aspartate codons in single and double combinations as shown in the figure (C).

3.2 | Phospho-mimetic replacement of S235 and S335 affects GTPase activity and interaction with GTP

The recombinant drFtsZ and its mutants' proteins were purified (Figure S1) and checked for secondary structure alteration, if any, using Circular Dichroism (CD) spectroscopy. All the mutant proteins produced the typical CD spectra, nearly identical to that of drFtsZ, with clear dips at 208 and 222 nm indicating that they all have α-helix secondary structures typical to the wild-type protein (Figure S1). The GTPase activity of S235 and S335 mutants were estimated using thin-layer chromatography and compared with drFtsZ (Figure 2A). Since the polymerization and GTPase activity of FtsZ requires a critical concentration of the protein, the activity was monitored at different protein concentrations in vitro for all the mutant forms. The replacement of S235 and S335 residues with aspartate has compromised the GTPase activity, *although* to different levels. For instance, the double phospho-mimetic mutant, S235DS335D (hereafter referred to as $FtsZ_{DD}$) showed a significant loss in GTPase activity (~3.0 ± 0.29-fold) compared to the wild type as well as the double phospho-ablative, S235AS335A (hereafter referred to as $FtsZ_{AA}$) (Figure 2B). Furthermore, the GTPase activity of the other single phospho-mimetic/ablative and the double mutants with one phospho-ablative residue and the other with phospho-mimetic residue was significantly low compared to the wild type. For instance, the single mutants like $FtsZ_{S235A}$, $FtsZ_{S335A}$, $FtsZ_{S235D}$ and $FtsZ_{S335D}$ showed respective GTPase activity by ~1.67 ± 0.32, ~1.62 ± 0.44, ~4.27 ± 0.16 and ~5.1 ± 0.188-fold less than the wild type. However, the reduction in GTPase activity in double mutants $FtsZ_{AD}$ and $FtsZ_{DA}$ was ~3.35 ± 0.58, ~3.46 ± 0.38 folds, respectively, as compared to drFtsZ at 5 μM. Interestingly, similar trends were obtained at 10 μM of protein concentration (data not shown). The loss of GTPase activity in mutants could be explained if these mutations have affected the wild-type interaction with GTP and/or the polymerization ability of these proteins.

The GTP binding assay was performed using 2′/3′-O-(N-methyl-anthraniloyl) guanosine 5′ triphosphate, trisodium salt (Mant-GTP) and 5 μM of wild-type and other mutant proteins as described in the method.

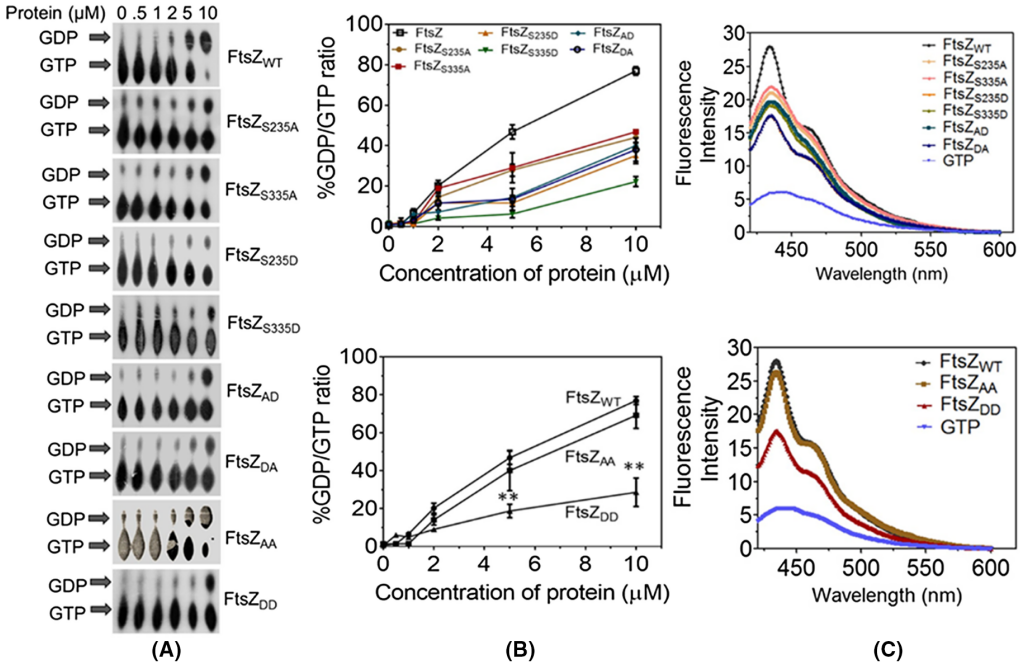

FIGURE 2 Characterization of phospho-mutants of drFtsZ for their GTPase activity and GTP binding. Purified recombinant $FtsZ_{WT}$ and its phospho-mutants as labelled in the figure were pre-incubated in polymerization (PB) buffer in a concentration-dependent manner. Reaction mixtures were spotted on PEI Cellulose F+ TLC sheets, dried and separated in a buffer system. TLC sheets were exposed to X-ray films and autoradiograms were developed and the conversion of GTP to GDP is marked with the arrows (A). Images were analysed using ImageJ. The levels of GTP and GDP were quantified from the data of two independent reproducible experiments. The percentage of GDP/GTP was calculated for each concentration of the different proteins and average with ±SD was plotted using GraphPad Prism (B). Nucleotide-binding assay of wild type and mutants of FtsZ was also performed. Emission spectra for mant-GTP alone and bound to wild-type and different mutants of FtsZ were recorded from 410 to 600 nm at an excitation wavelength of 355 nm. The color-coded lines represent the fluorescence signal from 100 nM mant-GTP in the presence of different proteins as mentioned in the figure (C).

The increase in fluorescence signals of Mant-GTP was observed in the presence of all the proteins. However, $FtsZ_{S235A}$, $FtsZ_{S335A}$, $FtsZ_{S235D}$, $FtsZ_{S335D,}$ $FtsZ_{AD}$, $FtsZ_{DA}$ and $FtsZ_{DD}$ mutants showed a relatively low increase in Mant-GTP fluorescence intensity compared to wild type and $FtsZ_{AA}$ (Figure 2C). This effect was more pronounced in the $FtsZ_{DD}$ mutant and surprisingly, there was no change when both the residues were replaced with alanine in $FtsZ_{AA.}$ These observations raised a strong possibility of S235 and S335 phosphorylation affecting the affinity of drFtsZ towards GTP suggesting that the phosphorylation of these residues seems to have affected the catalytic GTPase activity by affecting the nucleotide interaction with mutant forms of drFtsZ.

3.3 | Phospho-mimetic replacement of S235 and S335 affects the polymerization ability of drFtsZ

Since the phospho-mimetic replacement of S235 and S335 affected the GTPase activity and GTP interaction. Therefore, the effect of phospho-mimetic replacement of S235 and S335 on the polymerization of drFtsZ was examined using 90° angle dynamic light scattering (DLS), sedimentation assay and transmission electron microscopy. DLS analysis showed that the polymerization of the $FtsZ_{WT}$ and all the phospho-ablative mutants, including $FtsZ_{AA}$ was stimulated in the presence of GTP, while there was no change in the size of the polymers of phospho-mimetic-mutant proteins including $FtsZ_{DD}$ (Figure 3A). The light scattering signal remained near the baseline for phospho-mimetic mutants compared to wild-type and phospho-ablative mutants. Estimation of polymer size through sedimentation at higher speed showed similar results to those of DLS. Results showed that the amount of the phospho-mimetic mutants including $FtsZ_{DD}$ in the pellet was found to be nearly ~13.57 ± 2.48 times lesser than the drFtsZ, in the presence of both GTP and Mg^{2+}. Nearly similar results were obtained when $FtsZ_{DD}$ was incubated with GTP or Mg^{2+} alone. This indicated that unlike drFtsZ and phospho-ablative mutants, including $FtsZ_{AA,}$ the phospho-mimetic mutants do not form higher-order structures in the presence of GTP alone or GTP with Mg^{2+} (Figure 3B & Figure S2). Transmission electron microscopic studies also showed that the drFtsZ

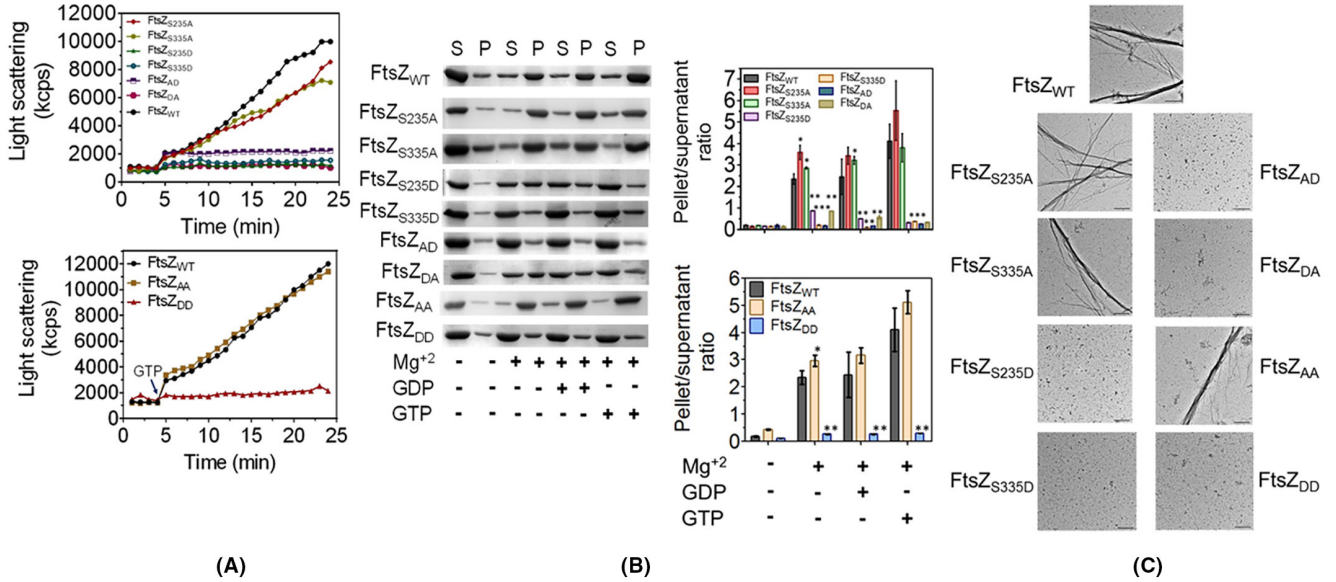

FIGURE 3 Monitoring of phospho-mutants of FtsZ for their polymerization abilities. Five micromolar of the purified recombinant $FtsZ_{WT}$ and other phospho-mutant proteins were preincubated in PB buffer only followed by the addition of GTP (shown by arrow) at 37°C for 5 min in a quartz cuvette and then the light scattering was recorded for 20 min at an interval of 30 s. Light scattering intensity in kilocounts per sec (kcps) was plotted against time using GraphPad Prism software for each protein as mentioned in the graph (A). Similarly, 5 μM of the purified recombinant FtsZ and phospho-mutant derivatives were preincubated in PB buffer supplemented with 5 mM $MgCl_2$, followed by the addition of 1 mM of GTP/GDP and incubated for 20 min at 37°C. Reaction mixtures were centrifuged and the pellet (P) and supernatant (S) fractions were separated and analysed on SDS-PAGE, stained with Coomassie brilliant blue. Images were analyzed using ImageJ. The ratio of pellet to supernatant was plotted using GraphPad software (B). For transmission electron microscopy, 5 μM of wild-type and mutant proteins were incubated in polymerization buffer (PB buffer; Tris–HCl, pH 7.6; 50 mM, KCl; 50 mM and $MgCl_2$; 1 mM) for 5 min at room temperature followed by the addition of 1 mM GTP and incubation at 37°C followed by mounting on carbon-coated TEM grids. The grids were observed using transmission electron microscope JEM-1400 (JEOL) transmission electron microscope with a magnification of 10,000× (Scale bar 500 nm) (C).

and phospho-ablative mutants including $FtsZ_{AA}$ can form higher-order polymeric structures, while phospho-mimetic derivatives, including $FtsZ_{DD}$ failed to produce higher-order polymeric structures and exist as small protofilaments (Figure 3C).

3.4 | Phospho-mimetic replacement of S235 and S335 altered the physiological behaviour of drFtsZ

The expression of translation fusion of drFtsZ (pDsZ[21]), $FtsZ_{AA}$ (pDsZAA) and $FtsZ_{DD}$ (pDsZDD) with GFP was ascertained in the *E. coli* cells using a confocal microscope. The $FtsZ_{AA}$-mutant protein formed the spiral-like cytoskeletal structures in the *E. coli* cells, mocking the phenotype of cells overexpressing drFtsZ (Figure 4A). The *E. coli* cells expressing drFtsZ and $FtsZ_{AA}$ have shown an elongated cell phenotype (Figure 4B). Earlier, a similar observation was reported in *E. coli* cells overexpressing their native FtsZ episomally.[37] Interestingly, unlike the wild-type and $FtsZ_{AA}$, the $FtsZ_{DD}$ expressing *E. coli* cells have shown normal foci appearance and shorter cell phenotype in comparison to cells expressing drFtsZ and $FtsZ_{AA}$ (Figure 4A,B). In *E. coli*, this phenotype has been attributed to the higher levels of recombinant FtsZ.[37] Therefore, the levels of drFtsZ, $FtsZ_{AA}$ and $FtsZ_{DD}$ proteins were measured in the *E. coli* cells expressing these proteins from the same vector under a similar promoter. All cell types including such as drFtsZ, $FtsZ_{AA}$ and $FtsZ_{DD}$ had nearly the same levels of FtsZ-GFP protein as detected by the GFP antibody (Figure S3A), indicating that mimicking phosphorylation in drFtsZ ($FtsZ_{DD}$) alters its classical behaviour at least in *E. coli*. In spite of the difference in morphology and the FtsZ cytoskeletal appearance, the cells expressed nearly the same levels of wild-type and phospho-mimetic mutants of FtsZ. This result clearly suggested that the cell elongation and spiral cytoskeleton FtsZ phenotypes are not only due to levels of proteins as suggested earlier rather also depend upon their functional states.

Subsequently, the localization pattern and dynamics of both drFtsZ ($FtsZ_{WT}$; pRGZGFP), $FtsZ_{AA}$ ($pRGZ_{AA}GFP$) and $FtsZ_{DD}$ ($pRGZ_{DD}GFP$) were monitored in *D. radiodurans* under normal conditions and after exposure to γ-radiation. These cells were observed using time-lapse microscopy. The localization and cellular dynamics of drFtsZ and its mutants were found to be different under

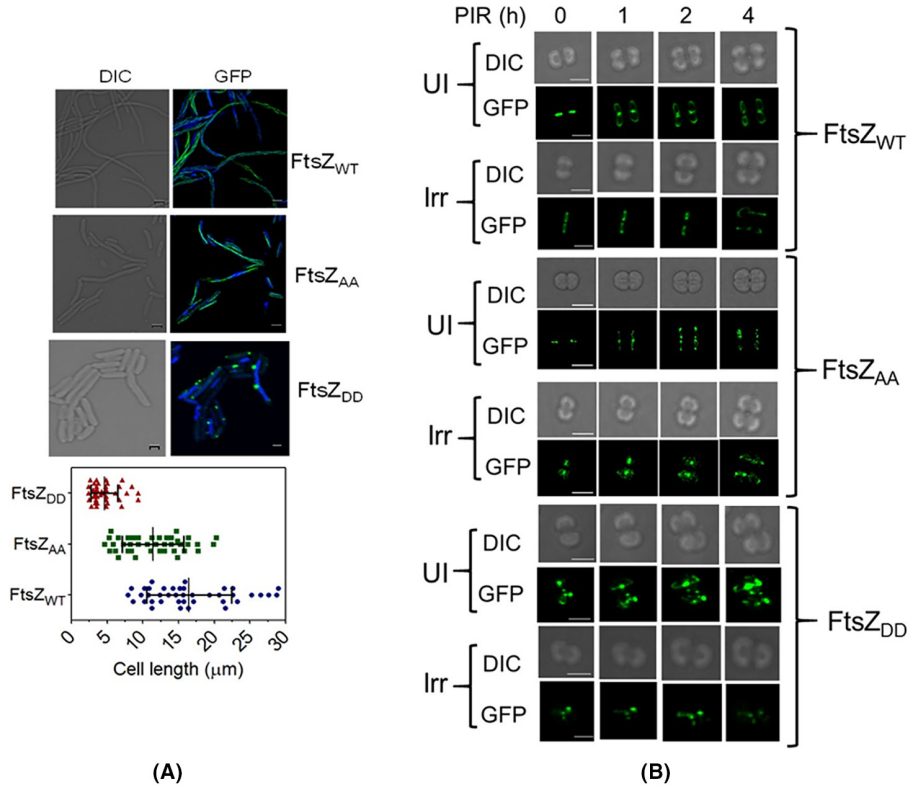

FIGURE 4 Effect of the mutations on drFtsZ localization dynamics and in vivo functions. For fixed cell imaging, the *Escherichia coli* cells expressing pDSZ ($FtsZ_{WT}$), pDsZAA ($FtsZ_{AA}$) and pDsZDD ($FtsZ_{DD}$) were fixed and observed using a confocal microscope Olympus IX83 inverted microscope equipped with an IX3SVR motorized platform. These cells were also stained with DAPI and observed to map the localization of FtsZ with respect to the genome. The image analysis was done using automated cellSens software. Data obtained were subjected to Student *t* test analysis using statistical programs of GraphPad Prism ($n = 200$). Scale bar denotes 2 μm (A). For time-lapse imaging of the cell growth and division process, cells in the exponential phase were exposed to a 6 kGy dose of γ-radiation, whereas the control cells were kept on ice. After **γ**-irradiation, both unirradiated (UI) and irradiated (Irr) cells expressing pRGZGFP ($FtsZ_{WT}$), $pRGZ_{AA}GFP$ ($FtsZ_{AA}$) and $pRGZ_{DD}GFP$ ($FtsZ_{DD}$) mounted on 2X-TYG agarose pad before imaging using confocal microscope Olympus IX83 inverted microscope. Air holes were designed in agarose pads to oxygenate the cells. The 3D images (Z planes were acquired every 400 nm) were acquired every 45–60 min for a period of 4–5 h using very low 488 nm laser power. Images were processed using the cellSens software and Adobe Photoshop 7.0.

normal and γ-stressed conditions. For instance, under normal conditions, the drFtsZ-ring formation was found to be perpendicular to the previous plane of cell division in a timescale that corresponds to 1–2 h PIR (Figure 4B) and the constriction of the cell envelope was evident by the closure and separation of Z-rings in the daughter cells in a timescale that corresponds to 4 h PIR (Figure 4B). However, when exposed to γ-radiation, the formation of Z-ring in the required plane was delayed and observed after nearly 4 h. Since drFtsZ undergoes phosphorylation during this timescale of PIR, a possibility of delayed Z-ring formation and dynamics due to phosphorylation of drFtsZ could be speculated. To answer it, the cells expressing both $FtsZ_{AA}$-GFP and $FtsZ_{DD}$-GFP were compared with drFtsZ under both types of growth conditions. Under normal conditions, cells expressing $FtsZ_{AA}$-GFP have the pattern of appearance and cellular growth as of the cells expressing drFtsZ; however, after γ-irradiation, the cells showed a delay in cell division, but the dynamics of $FtsZ_{AA}$ seemed to resume a bit early as shown by at 3 h PIR since the sites for phosphorylation were not present (Figure 4B). The cells expressing $FtsZ_{DD}$-GFP episomally showed a cell division pattern similar to the cells expressing wild-type protein episomally (Figure 4B). This result could be attributed to the dominant phenotype of chromosomally encoded drFtsZ over $FtsZ_{DD}$-GFP in the wild-type background. When exposed to γ-irradiation, both types of cells showed a similar trend in cell division, perhaps due to the normal copy of drFtsZ in the wild-type background. When we monitored the status of GFP variants of these proteins, amazingly, the $FtsZ_{DD}$-GFP expressing cells failed to form any new and active structures; instead, they produced an erratic pattern of $FtsZ_{DD}$-GFP localization at 4 h PIR (Figure 4B). Further, unlike the drFtsZ cells that got rescued from γ-irradiation effects in 4/5 h of the PIR, the $FtsZ_{DD}$ mutant failed to do so and continued to show an aberrant pattern of localization

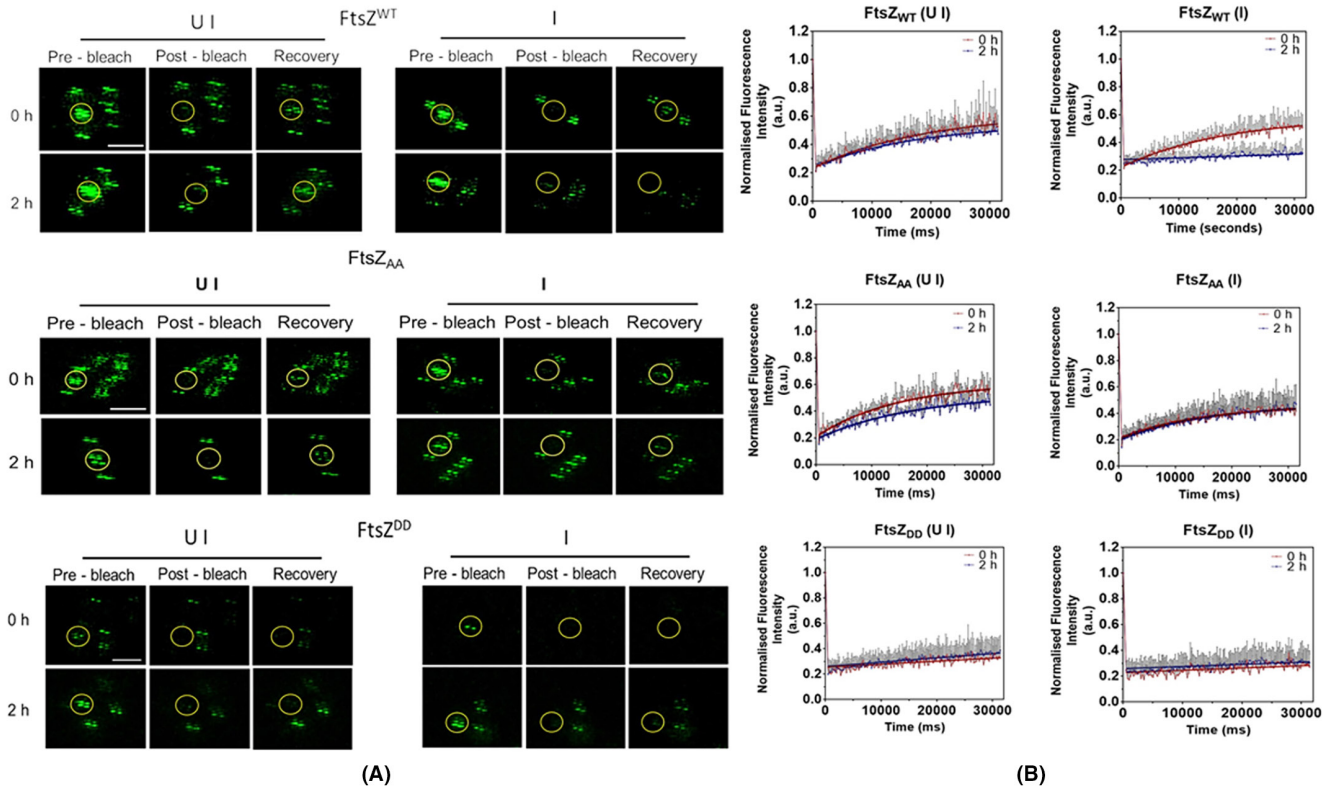

FIGURE 5 Mimicking phosphorylation mutation affects the recovery dynamics of drFtsZ. For FRAP microscopic analysis, the cells in the exponential phase were exposed to a 6 kGy dose of γ-radiation, whereas control cells were kept on ice. After γ-irradiation, both unirradiated (UI) and irradiated (Irr) cells expressing pRGZGFP ($FtsZ_{WT}$), $pRGZ_{AA}GFP$ ($FtsZ_{AA}$) and $pRG_{DD}GFP$ ($FtsZ_{DD}$) mounted on 2X-TYG agarose pad before imaging. The representative images of pre-bleach, bleach and recovery phase are also shown (A). FRAP measurements were made at room temperature. The region of interest was exposed to a laser bleach pulse of 35–45 ms followed by the acquisition of recovery for 30–40 s at low laser power. The fluorescence intensities in the bleached and other regions at each time point were extracted using the cellSens software and exported to Excel 2013. Recovery curves were plotted by performing a non-linear regression fit of the intensity of the bleached region over time using GraphPad Prism 6 software (B).

even after several hours of the PIR period. Since the differences in phenotype could be due to the difference in their plasmid copy number or the expression levels of FtsZ and its mutants in *D. radiodurans*, the cells episomally expressing GFP fusions of wild type and mutants' proteins were primarily checked for the level of recombinant proteins using antibodies against GFP and FtsZ. Results showed that the levels of FtsZ protein were largely the same across the variants (Figure S3B,C). These findings suggested that mimicking phosphorylation at S235 and S335 positions in drFtsZ by a γ-radiation responsive eSTPK (RqkA) alters the typical characteristics of FtsZ, and if this can arrest its dynamics in response to γ-radiation exposure could be hypothesized.

3.5 | Mimicking phosphorylation affected in vivo dynamics of drFtsZ

A possible effect of phosphorylation on drFtsZ dynamics after γ-radiation exposure was studied by the FRAP technique. Wild-type cells expressing the GFP fusion of both drFtsZ, $FtsZ_{AA}$ and $FtsZ_{DD}$ mutant were grown under normal (unirradiated) and gamma-stressed (irradiated) conditions. Earlier, we have shown that 0 and 2 h PIR cells showed contrasting phenotypes in terms of drFtsZ phosphorylation and growth arrest.[29] Therefore, the 0 and 2 h PIR cells were used for studying the effect of phosphorylation on the polymerization dynamics of drFtsZ and its mutants. These cells were examined microscopically and the FtsZ foci were studied for FRAP. The results showed that the drFtsZ foci were able to recover under normal conditions (Figure 5A,B). In response to γ-irradiation, the bleached foci of drFtsZ could recover at 0 h of PIR but not in 2 h of PIR cells suggesting that the phosphorylation of FtsZ that would have occurred between 2 and 3 h PIR under our experimental condition[29] seems to have affected its polymerization/depolymerization characteristics in vivo. Interestingly, the foci of $FtsZ_{AA}$ have shown recovery under both un-irradiated and irradiated conditions. Because the phospho-ablative mutant mimics the non-phosphorylated form, which is

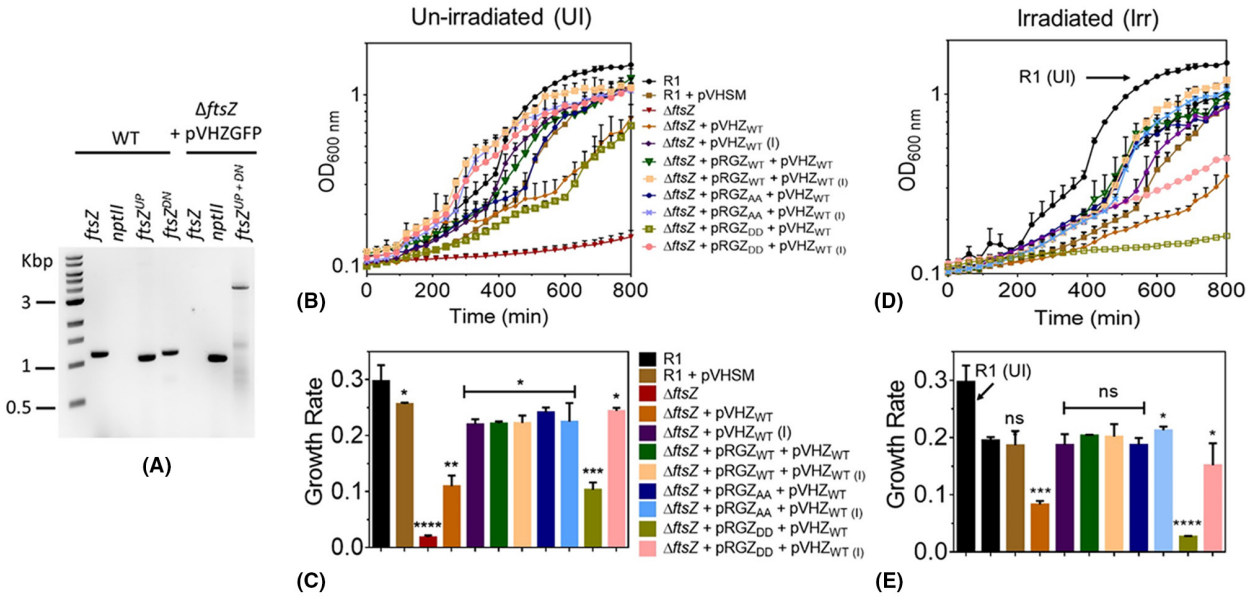

FIGURE 6 Phospho-mimetic mutant failed to support the cell growth. The plasmid pNKZ was linearized and transformed into the *D. radiodurans* cells harbouring pVHZGFP and transformants were scored in the presence of kanamycin and spectinomycin. The replacement of *ftsZ* with an antibiotic resistance marker gene (*nptII*) was confirmed by diagnostic PCR using primers as described in Table 1 *nptII* for the antibiotic resistance gene, *ftsZ* for the FtsZ-coding sequence, $ftsZ^{UP}$ and $ftsZ^{DN}$ for upstream and downstream sequences of *ftsZ*, respectively. The $ftsZ^{UP+DN}$ indicates the product of $ftsZ^{UP} + nptII + ftsZ^{DN}$ from the conditional null mutant (A). The wild-type and conditional null-mutant derivatives were monitored for their growth kinetics under normal conditions using a Synergy H1 multiplate reader. The wild-type strain (R1), R1 harbouring vector backbone of pVHSM (R1 + pVHSM), presumptive null mutant of *ftsZ* (Δ*ftsZ*) harbouring pVHZGFP (Δ*ftsZ* + $pVHZ_{WT}$), conditional null mutant of *ftsZ* (Δ*ftsZ* + $pVHZ^{WT}$) harbouring pRGZGFP ($pRGZ_{WT}$), $pRGZ_{AA}$GFP ($pRGZ_{AA}$) and $pRGZ_{DD}$GFP ($pRGZ_{DD}$) were monitored for their growth in the presence and absence of IPTG, where I indicates the induced status of the pVHZGFP in the corresponding strain as shown in the graph (B). Δ*ftsZ* failed to grow in the absence of an episomal copy of FtsZ and hence was omitted from the comparisons. The growth rate was calculated from the corresponding growth curve values and plotted using GraphPad Prism software (C). Similarly, the wild-type and conditional null-mutant derivatives were monitored for their growth kinetics after γ-irradiation using a Synergy H1 multiplate reader (D). The growth rate was calculated from the corresponding growth curve values and plotted using GraphPad Prism software (E).

attributed to the recovery under γ-irradiated condition, but the cells show delayed division due to the global effect of the irradiation as observed in Figure 4B. Notably, under both normal and γ-stressed growth conditions, the bleached foci corresponding to $FtsZ_{DD}$ protein did not recover (Figure 5A,B). This could imply that the FtsZ phosphorylation regulates the dynamics required for cells to undergo binary fission, and the possibility of regulation of the cell cycle arrest following γ-radiation exposure cannot be ruled out, at least in this bacterium.

3.6 | Phospho-mimetic mutant of drFtsZ failed to complement *ftsZ* loss in *D. radiodurans*

To understand the effect of S235 and S335 phosphorylation on the growth of *D. radiodurans*, we needed the null mutant of *ftsZ* for complementation studies. Since the homogeneous replacement of *ftsZ* with an expressing cassette of *nptII* could not be possible, the *ftsZ* conditional-null mutant (Δ*ftsZ*) was created in the presence of an episomal copy of drFtsZ. The homogenous replacement of the target sequence with *nptII* cassette was confirmed by diagnostic PCR (Figure 6A), and with *ftsZ*::*nptII* genotype having drFtsZ expressing under IPTG inducible promoter on pVHZGFP plasmid was obtained. These cells grew normally in the presence of IPTG and did not lose viability while they were debilitated in the absence of IPTG, and hereafter termed as *ftsZ* conditional-null mutant (Δ*ftsZ*). The effect of phospho-mimetic replacement of S235 and S335 on functional complementation in Δ*ftsZ* was monitored under normal (Figure 6B,C) and γ-radiation stressed conditions (Figure 6D,E). For that, the drFtsZ, $FtsZ_{AA}$ and $FtsZ_{DD}$ proteins were constitutively expressed in Δ*ftsZ* cells under *groESL* promoter from pRadgro derivatives (Table 1), and the growth of these cells was monitored in the presence and absence of IPTG (Figure 6B,C). The Δ*ftsZ* cells constitutively expressing drFtsZ and $FtsZ_{AA}$ from the plasmid grew normally and nearly similar to wild-type cells irrespective of the episomal expression of drFtsZ, suggesting that the basal expression of phospho-ablative

mutant could complement the normal growth of the Δ*ftsZ* cells. However, the Δ*ftsZ* cells constitutively expressing $FtsZ_{DD}$ grew slower in the absence of IPTG (possible leaky expression of drFtsZ), which was recovered to normal growth when these cells were induced with 5 mM IPTG for making drFtsZ episomally. Under γ-stressed conditions, the Δ*ftsZ* cells constitutively expressing drFtsZ, $FtsZ_{AA}$ showed a similar growth arrest as observed for the wild-type strain after γ-irradiation. However, the Δ*ftsZ* cells expressing $FtsZ_{DD}$ mutants showed debilitated growth upon γ-radiation exposure in the absence of IPTG (absence of wild-type drFtsZ). This indicated that the phospho-mimetic mutant of FtsZ ($FtsZ_{DD}$) has failed to complement drFtsZ loss in Δ*ftsZ* cells also when exposed to γ-radiation. As expected, these cells showed growth though slower, when drFtsZ was expressed episomally in the presence of IPTG (Figure 6D-E). These results suggested that mimicking the S235 and S335 phosphorylation in FtsZ has affected the post-irradiation recovery of Δ*ftsZ* cells compared to the cells expressing the wild-type FtsZ.

4 | DISCUSSION

FtsZ is a key protein in bacterial cell division, and one of its intrinsic properties that regulate bacterial growth is the GTP/Mg^{2+} supported polymerization/depolymerization dynamics. In response to DNA damage, the activity of FtsZ is attenuated by SOS proteins like SulA in *E. coli*,[14] YneA in *B. subtilis*,[15] Rv2719c in *M. tuberculosis*[16] and SidA in *C. crescentus*.[17] *D. radiodurans* is well known for its exceptional resistance to several DNA-damaging agents including γ-radiation. Cells exposed to γ-radiation show a nearly 4 h lag in growth, presumably until damaged DNA is repaired. During this time, there is no significant change in the levels of some cell division proteins, including FtsZ. Unlike other bacteria, this bacterium does not deploy LexA/RecA-type SOS mechanisms to control the cell cycle in response to DNA damage. However, it resists the lethal doses of γ-radiation and other DNA-damaging agents by undergoing both qualitative and quantitative changes in its genome's functions. These findings collectively argued in the favour of some alternate mechanism(s) of the DNA damage response and cell cycle regulation in this bacterium.

Post-translational modifications (PTMs) are known to play significant roles in the regulation of cellular dynamics, macromolecular interactions and stress-responsive gene expression in higher organisms.[38,39] Notably, the Ser/Thr (S/T) phosphorylation of proteins is the key regulatory mechanism of cell cycle regulation in eukaryotes. Recently, S/T phosphorylation has also been reported in bacterial proteins involved in cell division, genome maintenance and pathogenesis.[40] The S/T phosphorylation of DNA repair proteins like RecA has been demonstrated in *B. subtilis* grown under normal conditions.[41] The genome of *D. radiodurans* also encodes a few typical eukaryotic-type STPKs and one such STPK (RqkA) has been characterized for its role in radioresistance. The *rqkA* mutant was found to be hypersensitive to γ radiation and showed near-complete arrest of DSB repair.[26] RqkA could phosphorylate a number of deinococcal proteins including PprA, RecA, FtsZ and FtsA. The effect of S/T phosphorylation on the functions of DNA repair proteins (RecA and PprA) and radiation resistance has also been demonstrated in this bacterium.[26,42] Although, the S/T phosphorylation of drFtsZ and drFtsA by RqkA and their kinetic change during PIR has been reported,[29] the impact of such phosphorylation on the cell cycle regulation in response to DNA damage has not been shown yet. This study has brought forth some direct evidence to suggest that the phosphorylation of drFtsZ by RqkA has affected its intrinsic properties in vitro and cellular dynamics under both normal and γ-stressed conditions in vivo. We demonstrated that the replacement of phosphorylated serine's like S235 and S335 with aspartate reduces the GTPase activity by affecting GTP interaction with the protein. The polymerization ability of these mutants was severely compromised in vitro, which appears to be due to the loss of the GTP-binding ability of such proteins. The effect of S235 and S335 phosphorylation on the GTP-binding pocket of drFtsZ was studied in silico. The position of the GTP-binding pocket in drFtsZ was altered when S235 or S335 or both were replaced with phospho-mimetic residue (aspartate) (Figure S4A [i]). For instance, in drFtsZ, it was positioned in the region between 96 and 101 residues. Interestingly, in $FtsZ_{DD}$, the GTP-binding pocket got shifted to a region between 321 and 341 residues and became close to the IDP territory (Figure S4A [ii]). In the case of both single phospho-mimetic mutants, $FtsZ_{S235D}$ and $FtsZ_{S335D}$, the GTP binding pocket was also shifted to the region between 126 and 131 residues (Figure S4A [iii, iv]). FtsZ phosphorylation has been reported in a variety of bacteria including mycobacteria,[27] streptococci,[43] staphylococci[44] and *D. radiodurans*.[29] However, phosphorylation of FtsZ affecting cell cycle in response to DNA damage is first time demonstrated in *D. radiodurans*. The localization pattern of the phospho-mimetic mutant is found to be completely different from that of the phospho-ablative mutant and wild-type in both ex vivo and in vivo conditions, suggesting that mimicking phosphorylation has compromised the native functions of this protein. It has been previously demonstrated that phosphorylation of drFtsZ follows kinetics during PIR, with its highest levels during 2 h and 3 h PIR, which also coincides with the arrest of growth upon DNA damage. Therefore, a possibility

of FtsZ phosphorylation arresting the in vivo dynamics of the FtsZ-ring and thereby causing growth arrest can be hypothesized. The FRAP analysis of wild-type and phospho mutants clearly supported that the dynamics of phosphomimetic drFtsZ are arrested upon γ-radiation exposure. To the best of our knowledge, the involvement of S/T phosphorylation on FtsZ dynamics has not been shown before in any bacteria, and therefore, it offers a unique example of LexA/RecA independent cell cycle arrest through S/T phosphorylation in this bacterium.

In conclusion, this study has provided some evidence to suggest that the DNA damage response and cell cycle in response to γ-radiation are regulated by eukaryotic-type STPK (RqkA) in *D. radiodurans* that apparently lack the canonical SOS response as known in other bacteria. Independently, it has been shown that S/T phosphorylation of DNA repair proteins stimulates their functions and is needed for their support of radioresistance. Here, we have provided evidence that mimicking the phosphorylation of S235 and S335 of FtsZ causes the loss of its polymerization ability in vitro and the arrest of cellular dynamics in vivo. The arrest in the dynamics of wild-type FtsZ was observed in *D. radiodurans* in response to γ-radiation but its reversal was seen at a later phase of PIR. However, the phospho-mimetic mutant did not resume dynamics during the PIR period monitored under this study. These findings allow us to conclude that RqkA-mediated phosphorylation of S235 and S335 in drFtsZ in response to γ-radiation seems to be the key regulator of FtsZ functions and cell cycle progression in *D. radiodurans*. Furthermore, the phosphorylation of drFtsZ at S235 and S335 residues appears to be the key factor for growth arrest in response to γ-radiation exposure and DNA damage, at least in this bacterium.

AUTHOR CONTRIBUTIONS

Chaudhary Reema, Mishra Shruti and Maurya Ganesh K performed the research, acquired the data, analyzed and interpreted; Misra Hari and Rajpurohit Yogendra Singh conceived and designed the research, analysed and interpreted the data. All authors were involved in drafting and revising the manuscript.

ACKNOWLEDGEMENTS

The authors would like to thank Mrs Rimanshee Arya for her help with the Malvern Zetasizer and JASCO Spectrophotometer and Mr Shishu Kant Suman for helping in studies using fluorescent-labelled nucleotides. Reema Chaudhary is grateful to the Department of Atomic Energy, India for her fellowship.

CONFLICTS OF INTEREST

The authors declare that they have no conflict of interest.

DECLARATION

This work has also been a part of doctoral thesis submitted to HBNI (A Department of Atomic Energy - Deemed to be University, Mumbai, India) by Dr. Reema Chaudhary.

ORCID

Hari S. Misra https://orcid.org/0000-0002-9349-1229

REFERENCES

1. Adams DW, Errington J. Bacterial cell division: assembly, maintenance and disassembly of the Z ring. *Nat Rev Microbiol*. 2009;7:642-653.
2. Haeusser DP, Margolin W. Splitsville: structural and functional insights into the dynamic bacterial Z ring. *Nat Rev Microbiol*. 2016;14:305-319.
3. Du S, Lutkenhaus J. At the heart of bacterial cytokinesis: the Z ring. *Trends Microbiol*. 2019;27:781-791.
4. De Boer P, Crossley R, Rothfield L. The essential bacterial cell-division protein FtsZ is a GTPase. *Nature*. 1992;359:254-256.
5. Bramhill D, Thompson CM. GTP-dependent polymerization of *Escherichia coli* FtsZ protein to form tubules. *Proc Nat Acad Sci*. 1994;91:5813-5817.
6. Oliva MA, Cordell SC, Löwe J. Structural insights into FtsZ protofilament formation. *Nat Struct Mol Biol*. 2004;11:1243-1250.
7. Wagstaff JM, Tsim M, Oliva MA, et al. A polymerization-associated structural switch in FtsZ that enables treadmilling of model filaments. *MBio*. 2017;8:e00254-e00217.
8. Lutkenhaus J. Assembly dynamics of the bacterial MinCDE system and spatial regulation of the Z ring. *Annu Rev Biochem*. 2007;76:539-562.
9. Erickson HP, Osawa M. FtsZ constriction force–curved protofilaments bending membranes. *Prokaryotic Cytoskeletons*. Springer; 2017:139-160.
10. Bi E, Lutkenhaus J. Cell division inhibitors SulA and MinCD prevent formation of the FtsZ ring. *J Bacteriol*. 1993;175:1118-1125.
11. Dajkovic A, Mukherjee A, Lutkenhaus J. Investigation of regulation of FtsZ assembly by SulA and development of a model for FtsZ polymerization. *J Bacteriol*. 2008;190:2513-2526.
12. Chen Y, Milam SL, Erickson HP. SulA inhibits assembly of FtsZ by a simple sequestration mechanism. *Biochemistry (ACS)*. 2012;51:3100-3109.
13. Bisson-Filho AW, Discola KF, Castellen P, et al. FtsZ filament capping by MciZ, a developmental regulator of bacterial division. *Proc Nat Acad Sci*. 2015;112:E2130-E2138.
14. Mukherjee A, Cao C, Lutkenhaus J. Inhibition of FtsZ polymerization by SulA, an inhibitor of septation in *Escherichia coli*. *Proc Nat Acad Sci*. 1998;95:2885-2890.
15. Kawai Y, Moriya S, Ogasawara N. Identification of a protein, YneA, responsible for cell division suppression during the SOS response in *Bacillus subtilis*. *Mol Microbiol*. 2003;47:1113-1122.
16. Chauhan A, Lofton H, Maloney E, et al. Interference of *Mycobacterium tuberculosis* cell division by Rv2719c, a cell wall hydrolase. *Mol Microbiol*. 2006;62:132-147.
17. Modell JW, Hopkins AC, Laub MT. A DNA damage checkpoint in *Caulobacter crescentus* inhibits cell division through a direct interaction with FtsW. *Genes Dev*. 2011;25:1328-1343.
18. Battista JR. Radiation resistance: the fragments that remain. *Curr Biol*. 2000;10:R204-R205.

19. Cox MM, Battista JR. *Deinococcus radiodurans*—the consummate survivor. *Nat Rev Microbiol*. 2005;3:882-892.
20. Slade D, Radman M. Oxidative stress resistance in *Deinococcus radiodurans*. *Microbiol Mol Biol Rev*. 2011;75:133-191.
21. Modi KM, Tewari R, Misra HS. FtsZDr, a tubulin homologue in radioresistant bacterium *Deinococcus radiodurans* is characterized as a GTPase exhibiting polymerization/depolymerization dynamics in vitro and FtsZ ring formation in vivo. *Int J Biochem Cell Biol*. 2014;50:38-46.
22. Liu Y, Zhou J, Omelchenko MV, et al. Transcriptome dynamics of *Deinococcus radiodurans* recovering from ionizing radiation. *Proc Nat Acad Sci*. 2003;100:4191-4196.
23. Tanaka M, Earl AM, Howell HA, et al. Analysis of *Deinococcus radiodurans*'s transcriptional response to ionizing radiation and desiccation reveals novel proteins that contribute to extreme radioresistance. *Genetics*. 2004;168:21-33.
24. Basu B, Apte SK. Gamma radiation-induced proteome of *Deinococcus radiodurans* primarily targets DNA repair and oxidative stress alleviation. *Mol Cell Proteomics*. 2012;11(1): M111.011734.
25. Narumi I, Satoh K, Kikuchi M, et al. The LexA protein from *Deinococcus radiodurans* is not involved in RecA induction following γ irradiation. *J Bacteriol*. 2001;183:6951-6956.
26. Rajpurohit YS, Misra HS. Characterization of a DNA damage-inducible membrane protein kinase from *Deinococcus radiodurans* and its role in bacterial radioresistance and DNA strand break repair. *Mol Microbiol*. 2010;77:1470-1482.
27. Thakur M, Chakraborti PK. GTPase activity of mycobacterial FtsZ is impaired due to its transphosphorylation by the eukaryotic-type ser/Thr kinase, PknA. *J Biol Chem*. 2006; 281(52):40107-40113.
28. Schäefer M, Schmitz C, Facius R, et al. Systematic study of parameters influencing the action of rose Bengal with visible light on bacterial cells: comparison between the biological effect and singlet-oxygen production. *Photochem Photobiol*. 2000;71:514-523.
29. Maurya GK, Modi K, Banerjee M, Chaudhary R, Rajpurohit YS, Misra HS. Phosphorylation of FtsZ and FtsA by a DNA damage-responsive ser/Thr protein kinase affects their functional interactions in *Deinococcus radiodurans*. *mSphere*. 2018;3:e00325 -e00318.
30. Weiss DS, Chen JC, Ghigo JM, Boyd D, Beckwith J. Localization of FtsI (PBP3) to the septal ring requires its membrane anchor, the Z ring, FtsA, FtsQ, and FtsL. *J Bacteriol*. 1999;181:508-520.
31. Misra HS, Khairnar NP, Kota S, Shrivastava S, Joshi VP, Apte SK. An exonuclease I-sensitive DNA repair pathway in *Deinococcus radiodurans*: a major determinant of radiation resistance. *Mol Microbiol*. 2006;59:1308-1316.
32. Chaudhary R, Kota S, Misra HS. DivIVA regulates its expression and the orientation of new septum growth in *Deinococcus radiodurans*. *J Bacteriol*. 2021;203:e00163-e00121.
33. Schaffner-Barbero C, Gil-Redondo R, Ruiz-Avila LB, et al. Insights into nucleotide recognition by cell division protein FtsZ from a mant-GTP competition assay and molecular dynamics. *Biohemistry (ACS)*. 2010;49:10458-10472.
34. Maurya GK, Kota S, Kumar NN, Tewari R, Misra HS. ParA proteins of secondary genome elements crosstalk and regulate radioresistance through genome copy number reduction in *Deinococcus radiodurans*. *Biochem J*. 2019;476:909-930.
35. Charaka VK, Misra HS. Functional characterization of the role of the chromosome I partitioning system in genome segregation in *Deinococcus radiodurans*. *J Bacteriol*. 2012;194:5739-5748.
36. Anderson DE, Gueiros-Filho FJ, Erickson HP. Assembly dynamics of FtsZ rings in Bacillus subtilis and *Escherichia coli* and effects of FtsZ-regulating proteins. *J Bacteriol*. 2004;186(17):5775-5781.
37. Dai K, Lutkenhaus J. The proper ratio of FtsZ to FtsA is required for cell division to occur in *Escherichia coli*. *J Bacteriol*. 1992;174:6145-6151.
38. Yakubu RR, Weiss LM, Silmon de Monerri NC. Post-translational modifications as key regulators of apicomplexan biology: insights from proteome-wide studies. *Mol Microbiol*. 2018;107(1):1-23.
39. Ivarsson Y, Jemth P. Affinity and specificity of motif-based protein–protein interactions. *Curr Opin Struct Biol*. 2019;54:26-33.
40. Rajpurohit YS, Sharma DK, Misra HS. Involvement of serine/threonine protein kinases in DNA damage response and cell division in bacteria. *Res Microbiol*. 2022;173(1-2):1038833.
41. Bidnenko V, Shi L, Kobir A, et al. *Bacillus subtilis* serine/threonine protein kinase YabT is involved in spore development via phosphorylation of a bacterial recombinase. *Mol Microbiol*. 2013;88(5):921-935.
42. Rajpurohit YS, Misra HS. Structure-function study of deinococcal serine/threonine protein kinase implicates its kinase activity and DNA repair protein phosphorylation roles in radioresistance of *Deinococcus radiodurans*. *Int J Biochem Cell Biol*. 2013;45:2541-2552.
43. Giefing C, Jelencsics KE, Gelbmann D, Senn BM, Nagy E. The pneumococcal eukaryotic-type serine/threonine protein kinase StkP co-localizes with the cell division apparatus and interacts with FtsZ in vitro. *Microbiol*. 2010;156(6):1697-1707.
44. Huemer M, Shambat SM, Pereira S, et al. Ser/Thr phosphoregulation by PknB and Stp mediates bacterial quiescence and antibiotic persistence in Staphylococcus aureus. *BioRxiv*. 2021. doi:10.1101/2021.05.06.442895

SUPPORTING INFORMATION

Additional supporting information can be found online in the Supporting Information section at the end of this article.

How to cite this article: Chaudhary R, Mishra S, Maurya GK, Rajpurohit YS, Misra HS. FtsZ phosphorylation brings about growth arrest upon DNA damage in *Deinococcus radiodurans*. *FASEB BioAdvances*. 2023;5:27-42. doi: 10.1096/fba.2022-00082